Antenna design and channel modeling in the BAN context—part I: antennas

annals of telecommunications - annales des télécommunications

ISSN 0003-4347
Volume 66
Combined 3-4

Ann. Telecommun. (2011) 66:139-155
DOI 10.1007/s12243-010-0237-4

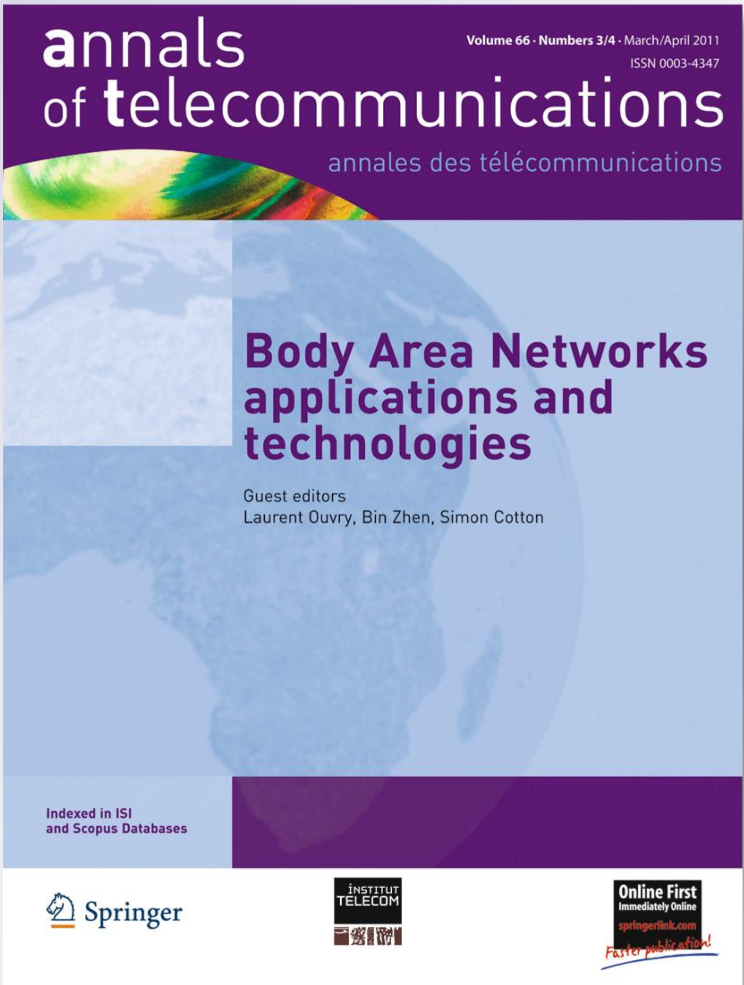

Ann. Telecommun. (2011) 66:139–155
DOI 10.1007/s12243-010-0237-4

Antenna design and channel modeling in the BAN context—part I: antennas

Christophe Roblin · Jean-Marc Laheurte · Raffaele D'Errico · Azeddine Gati · David Lautru · Thierry Alvès · Hanae Terchoune · Farid Bouttout

Received: 23 December 2009 / Accepted: 13 December 2010 / Published online: 19 January 2011

Abstract The first results achieved in the French ANR (National Research Agency) project BANET (Body Area NEtwork and Technologies) are presented (Part I). This project mainly deals with the antenna design in the context of Body Area Networks applications and channel characterization. General conclusions are drawn on the body impact on the antenna performance for *on–on* and *in–on* communications (Medical Implant Communication Systems). Narrow-band and ultra-wideband contexts are addressed both numerically and experimentally, and it is shown that design questions are significantly different for each case, leading to different constraints and guidelines. For narrow-band antennas, an alternative and original approach of desensitization using ferrite sheets is proposed and compared to classical techniques based on ground-plane screening. The characterization of numerical phantoms is also analyzed with narrow-band canonical antennas. For the specific *on–on* scenario, morphologies and electrical properties of the human tissues are also included in the topics of interest. For ultra-wideband antennas, focus is put on planar balanced designs, notably to reduce harmful "cable effects" occurring during the antenna characterization or the channel sounding. For both types of antennas, the main parameter under study is the distance to the body, which has a significant influence.

C. Roblin (✉)
ENSTA Paris-Tech,
32, Bd. Victor,
75739, Paris cedex 15, France
e-mail: christophe.roblin@ensta.fr
URL: www.ensta.fr

J.-M. Laheurte · T. Alvès
ESYCOM, Université Paris-Est Marne-La-Vallée,
5 Bd Descartes, Champs-sur-Marne,
77454, Marne La Vallée, France

J.-M. Laheurte
e-mail: laheurte@univ-mlv.fr
URL: www.esycom.univ-mlv.fr

T. Alvès
e-mail: talves@univ-mlv.fr
URL: www.esycom.univ-mlv.fr

R. D'Errico
CEA-Leti,
17, Avenue des Martyrs,
38054, Grenoble cedex 9, France
e-mail: raffaele.derrico@cea.fr
URL: www-leti.cea.fr

A. Gati · H. Terchoune
Orange Lab,
38-48, rue du Général Leclerc,
92794, Issy les Moulineaux, France

A. Gati
e-mail: azeddine.gati@orange-ftgroup.com

H. Terchoune
e-mail: hanae.terchoune@orange-ftgroup.com

D. Lautru · F. Bouttout
UPMC, Université Paris 06,
UR2, L2E, BC 252, 4 place Jussieu,
75005, Paris, France

D. Lautru
e-mail: david.lautru@upmc.fr
URL: http://www.l2e.upmc.fr

F. Bouttout
e-mail: f.bouttout@gmail.com
URL: http://www.l2e.upmc.fr

Keywords Body area network · Antenna · Input impedance · Total efficiency · Radiation pattern · Antenna miniaturization · UWB · Body absorption · Human tissues permittivity · Medical implants · MICS · On-body channel · In on-body channel

1 Overview

Wireless Body Area Networks (WBANs) are now recognized as promising candidates for various potential (and already existing) applications in the domains of health, surveillance, monitoring, sport, multimedia, entertainment, data transfer, etc. As the corresponding components and systems are embedded—and actually mainly body worn—the design constraints are particularly stringent: low power consumption is required for demanding applications requiring autonomy (e.g., medical surveillance), surety and safety are mandatory for vital applications, radiations are subject to regulatory limits for public health and coexistence reasons, and size, aspect ratio, and weight should be carefully dimensioned. All these constraints are intimately related to the acceptability by the future consumers. In particular, the reduced size constraint on sensors, actuators, and terminals is stringently reported on the antenna design. Furthermore, a detailed knowledge of the BAN propagation channel (which is intimately related to antenna/body interactions) is required to analyze and design properly systems at the physical interface (PHY), media access control (MAC), and networking levels.

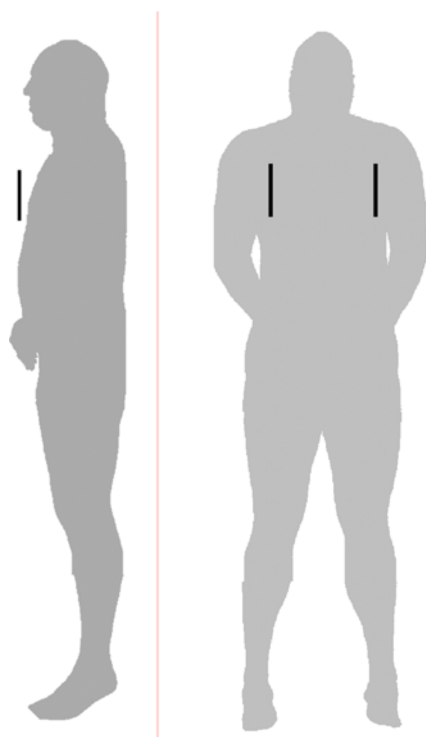

Fig. 1 Half-wave dipoles on the visible human model

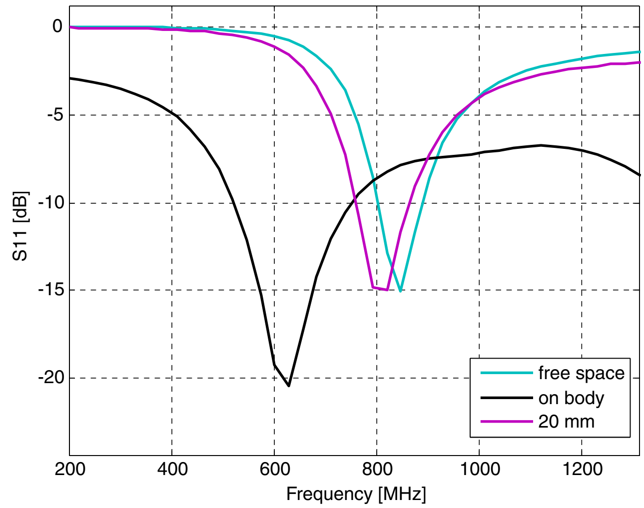

Fig. 2 Reflection coefficient of a dipole antenna placed on the left side of the chest directly on the body and at 20 mm from the body

In the context of WBANs, this paper deals with, first in part I, the analysis of the physical phenomena affecting the behavior of antennas and their design, and second in part II [1], the characterization and modeling of the on-body radio channel, namely CM3 in the IEEE 802.15.6 definition [2].

2 Introduction

To date, very few investigations have been performed on antennas specifically designed for BANs but many studies exist on applications facing similar constraints as BAN ones, i.e., miniaturization, low-profile and hostile environments. Among them, antennas integrated on clothing are widely documented. Published work on body-worn antennas for integration into clothing includes [3–5] which present linearly polarized fabric-based patch antennas and [6, 7] which describe a circularly polarized design. Fabric antennas have also been combined with electromagnetic

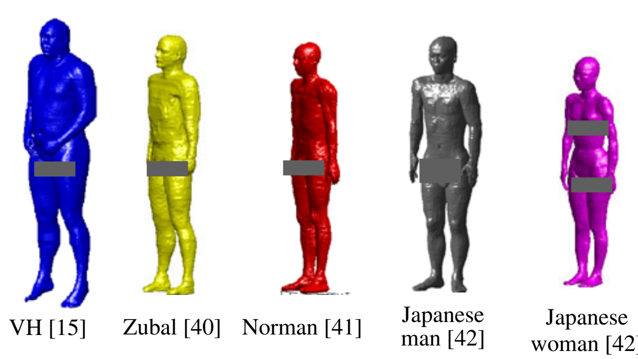

Fig. 3 Virtual phantoms with various morphologies

Table 1 Weight and height for the five models

Phantom	Weight (kg)	Height (m)	BMI (kg/m^2)	Radiation efficiency (%)
Visible human	106	1.82	32.0	37.58
Zubal	82	1.75	26.8	46.85
Norman	65.6	1.74	21.7	49.06
Japanese man	67	1.73	22.4	38.41
Japanese woman	53	1.61	20.4	31.45

band gap structures as reported in [8] for use in the 2.4- and 5-GHz bands. Button [9] and dielectric [10] antennas are also good candidates for ultra-wideband (UWB) applications as their radiation characteristics match the field structure of the creeping waves propagating along the body. But direct integration of antennas into clothing could be preferred as external devices might not be economically and practically viable.

The human body–antenna interaction topic has been for example studied in [11], investigating the performance of a body-worn planar inverted-F antenna (PIFA). In [12], an analysis of the influence of antenna positioning on the body have been carried out for several 2.4-GHz antennas such as monopole, patch, patch array, and loop. The radio link performance has been assessed with path gain measurements between two on-body antennas for various body postures. Results show that for most of the cases, the monopole–monopole combination gives the better link budget. In [13], a comparison of the performance of two antennas (a "printed horn shaped self-complementary antenna" and a "planar inverted cone antenna") in the characterisation of the on–on UWB channels shows that the former gives lower mean channel rms delay spread when propagation along the body (creeping waves) is dominant, whereas the latter present lower PL. In [14], the transmission of UWB antennas with omnidirectional, directional, and pattern diversity radiation characteristics has been experimentally characterized by placing them on or in close proximity to the human body.

The purpose of this paper is first to fully analyze the influence of the distance between the antenna and the body surface in the narrow-band and the UWB contexts for various antenna characteristics (resonant frequency, efficiency, bandwidth). It is demonstrated that different perspectives must be considered for narrow-band and UWB applications. As the overall approach is "application-oriented", hence "scenario-based", the frequency bands considered in this paper are the license-free bands 800–900 MHz (e.g., short-range devices, UHF, RFID, LTE, and 4 G), 2.4 GHz (e.g., ISM band including Bluetooth, WiFi and DCT), and around 400 MHz (Medical Implant Communication Service). For UWB antennas, the full 3.1–10.6 GHz is considered.

In section 3, some fundamental considerations on the influence of the body on antenna characteristics are pointed out. Then, the paper addresses BAN narrow-band antennas in section 4, whereas UWB radiating elements are discussed in section 5.

In sub-section 4.1 the influence of the antenna-to-body distance is investigated in simulation with the finite-difference time-domain (FDTD) method using canonical dipoles on numerical phantoms which include morphological characteristics. Then, various types of miniaturized planar antennas are implemented and tested experimentally in sub-section 4.2. In order to reduce the body influence, an

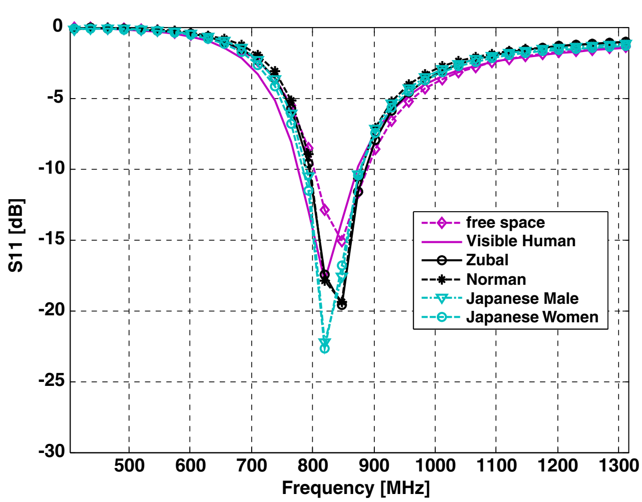

Fig. 4 Reflection coefficient of the dipole (distance δ=25 mm)

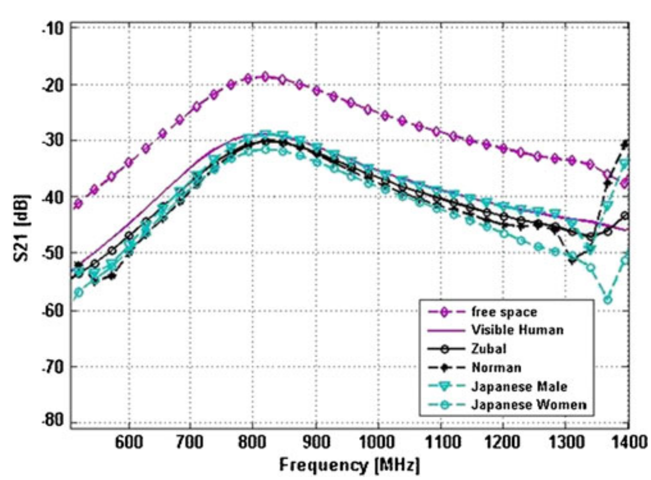

Fig. 5 Path gain $|S_{21}|$ as a function of the frequency

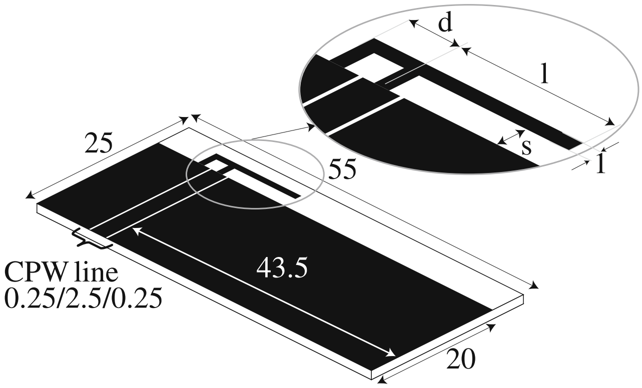

Fig. 6 IIFA topology [37]. Dimensions of the antenna are: s=2 mm, l=10.5 mm and d=3.5 mm

original electromagnetic desensitization technique using polymeric ferrite sheets is also presented.

In–on applications are considered in sub-section 4.3 for embedded loop antennas in the Medical Implant Communication Service (MICS) band around 402–405 MHz. This study points out the very low radiation efficiencies (<0.1%) resulting from the considerable power absorption due to human tissues surrounding the antenna and the impact of the depth of the implanted antenna on the path loss.

In section 5, several types of UWB antennas are firstly compared in terms of transmission and matching showing quite different performance depending on the frequency bands. In order to limit the parasitic effect of radio frequency (RF) cables located in the surrounding of the body, two balanced antennas are fully characterized and proposed as candidates for BAN channel sounding.

3 Considerations on antenna-human body interactions

The effective conductivity and relative permittivity of the human tissues strongly differ from free space. Therefore, the body modifies the antenna characteristics by shifting its resonant frequency, detuning its impedance matching,

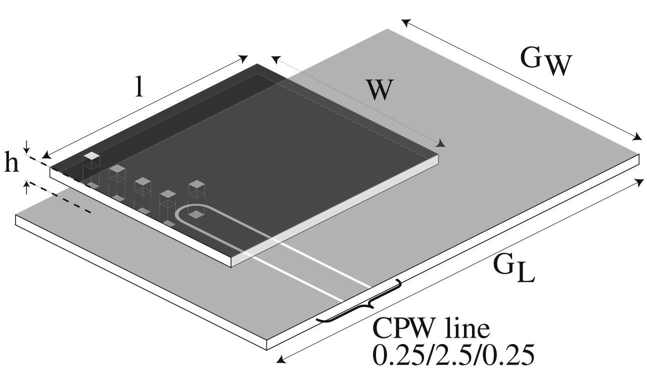

Fig. 7 PIFA topology [38]. Dimensions are: h=3.2 mm, l=20.6 mm, W=18 mm, G_w=25 mm and G_L=37 mm

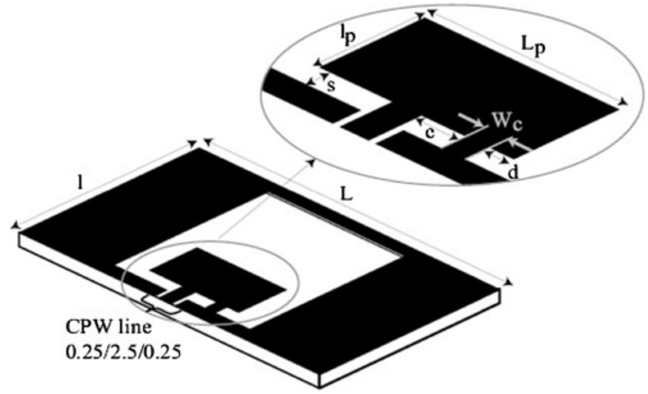

Fig. 8 CWPA topology [39]. Dimensions are: l_p=10.5 mm, L_p=13 mm, L=32 mm, l=24 mm, W_c=2 mm, s=0.7 mm, e=1 mm, d=2 mm

reducing its efficiency, and affecting its radiation pattern. This makes the design of narrow-band antennas particularly stringent. Furthermore, the strong dispersion of the electrical properties of human tissues is also a challenge for the design of numerical and real wideband phantoms which are widely used, both for the analysis of the behavior of antennas and their design, and for the characterization of the propagation channel.

The antenna performance is also related to the nature of the modes of propagation around the body (creeping waves, free-space radiation, reflections from surrounding objects) and the scenarios under consideration (hip to chest, hip to wrist, hip to ankle, chest to back, etc.). For on-body communications, minimal off-body radiation and maximal coupling between body-worn devices are normally required, although it could be possible to take advantage of off-body reflections by collecting additional energy (coming back from the environment) using more complex receivers such as RAKEs in UWB applications.

The strong influence of the proximity of a human subject on the behavior of on-body (or "body-worn") antennas—considering the frequency range for which the energy does not penetrate deeply in the body (say for simplicity above ~1 GHz)—appears significantly differently in the UWB and narrow-band cases. In both cases, the near-field coupling to the body modifies the antenna currents, impacting the input matching, and induces energy absorption, often significantly. However, in the narrow-band case studied in section 4, the dominant effect, and major drawback, is the shift of the resonance frequency causing mismatch (sometimes strongly), resulting in the collapse of the total efficiency (defined as the ratio of the radiated power to the incident power at the antenna input terminal[1]). This definition includes losses inside the body, not only in the antenna. Conversely, in the UWB case, the proximity of the body often improves the

[1] $\eta = \left(1 - |S_{11}|^2\right)\eta_{\mathrm{rad}}$, where η_{rad} is the radiation efficiency.

Table 2 Comparison of antenna performances

Antenna (f_r = 2.4GHz)	h (mm)	Relative Resonant Frequency Shift (%)		BW_{-10dB} (MHz)		Gain (dB)	Efficiency (%)	
		Measured	Simulated	Measured	Simulated	Simulated	Measured	Simulated
PIFA 	Free Space	--	--	123	100	3.4	90	92
	At 4 mm	1.1	1.2	187	190	0.6	--	39.5
IIFA 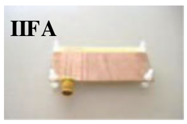	Free Space	--	--	821	820	3.2	95	97
	At 4 mm	32	22.5	686	690	-1.2	--	13.6
CWPA 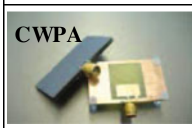	Free Space	--	--	130	120	2.3	97	91
	At 4 mm	17	5.3	950	110	-1.3	--	27.4

matching (generally increasing the bandwidth) for two reasons: first—but this is a very general effect—losses favor the matching (lowering $|S_{11}|$ more or less as a whole); second, the high permittivity of the human tissues, acting as a sort of additional substrate (in particular for planar tangent antennas without "screening isolation"), tends to shift-down the band.

The consequence in the narrow-band case is that much attention should be paid first to the matching aspects. In the UWB case, even though impedance matching is of major importance, the true performance indicator for antenna comparison purpose—aiming eventually the channel characterization and radio link performance—should be found directly in the transmission characteristics. UWB issues are addressed in section 5.

4 BAN antennas in a narrow-band context

4.1 Body influence on dipole antennas

In this section, the influence of the distance δ between the body and a half-wavelength dipole is emphasized with the help of a FDTD simulator and high–frequency structure simulator (HFSS). The frequencies under consideration are of practical interest in the 800–900-MHz band.

In a first study shown in Fig. 1, simulations have been carried out using the chest of the 3D body phantom "Visible Human" segmented by Brooks Air Force laboratories [15]. The chest is heterogeneous and composed of 38 different tissues. The antenna—horizontal half-wave dipole (~16.7 cm long) parallel to the body surface—is placed directly on the chest (δ=0) and slightly above it (δ= 20 mm). The detuning due to the presence of the body is emphasized in Fig. 2. The proximity of the body strongly detunes the antenna, lowering the resonance frequency with respect to that of free space. For δ=0, the frequency is shifted by about 200 MHz, i.e., ~25% of the nominal frequency. The fact that the reflection coefficient curve remains much below 0 dB below and above resonance indicates poor efficiency performances. For δ=20 mm, the frequency is shifted by about 40 MHz, i.e., ~5% of the nominal frequency.

Absorbed and radiated powers are evaluated relatively to the power accepted in the excitation gap taking into account the scattering parameters. For δ=0, the absorbed power is

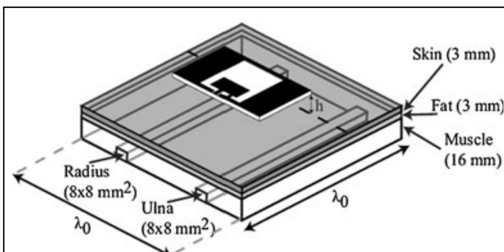

Tissue	Conductivity S/m	Relative Permittivity	Loss Tangent
Bone Cortical	0.39	11.4	0.25
Fat	0.11	5.3	0.14
Dry Skin	1.60	42.8	0.27
Muscle	1.74	52.7	0.24

Fig. 9 Human arm phantom with associated dielectric properties of human tissues

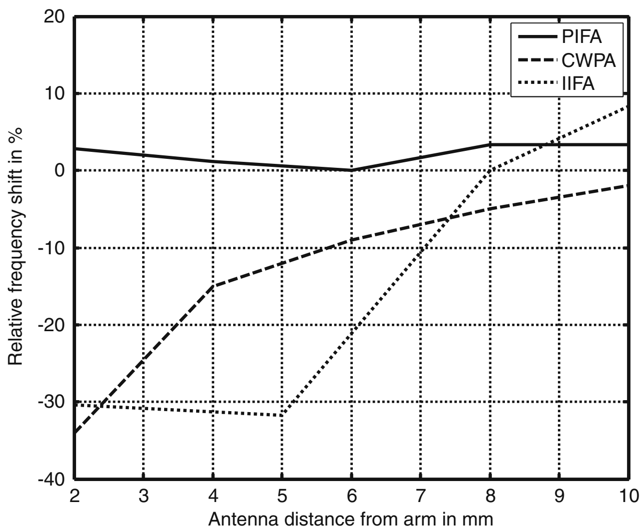

Fig. 10 Relative shift of the resonant frequency as a function of the antenna distance from the body for different antennas

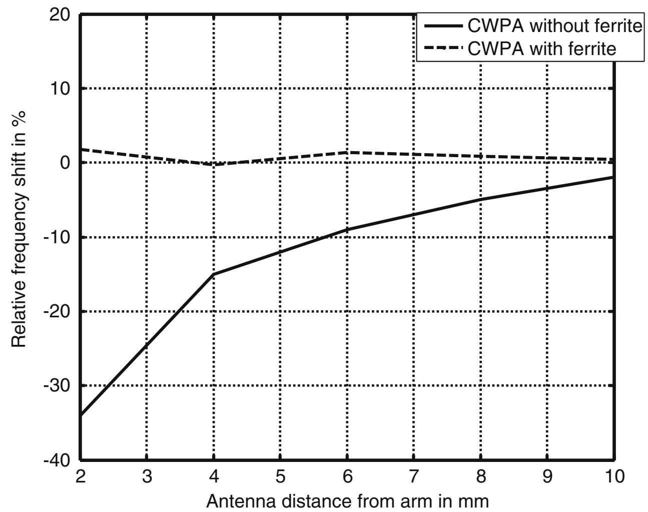

Fig. 12 Frequency shift improvement with ferrite polymer for the CWPA

higher than 90% of the accepted power and the radiated power evaluated using the far field is less than 10% of the accepted power. When the same dipole is placed at δ= 20 mm from the body surface, i.e., δ/λ_0=0.05 where λ_0 is the wavelength in free space, the absorbed power is about 65% while 35% is radiated in far field. We conclude that most of the accepted power is absorbed by the body for small distances between the body and the antenna.

In a second study, the antenna performance is determined for five different numerical human body models (Fig. 3)—or *virtual anthropomorphic phantoms*—presenting significantly different morphologies (Table 1). The mean morphological characteristics of the models are a weight of 76 kg (with an important standard deviation of 18.5 kg) and a height of 1.73 m (with a standard deviation of 7 cm).

The curves are given for a constant distance δ=25 mm from the body around 800 MHz. This distance was chosen higher than 20 mm because of the detuning problem shown in Fig. 2 and also to avoid the positioning problems with the Japanese Women phantom chest.

First, the reflection coefficient S_{11} is simulated under free-space conditions and for the five models as shown in Fig. 4. Resonant frequencies are nearly the same for all cases and do not vary significantly from free space. The return loss is greater than 10 dB in the considered 400-MHz band.

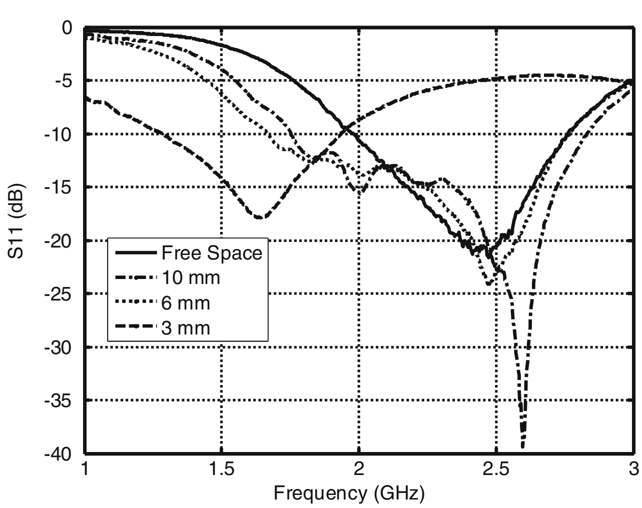

Fig. 11 IIFA matching as a function of the frequency for various antenna distances to the body

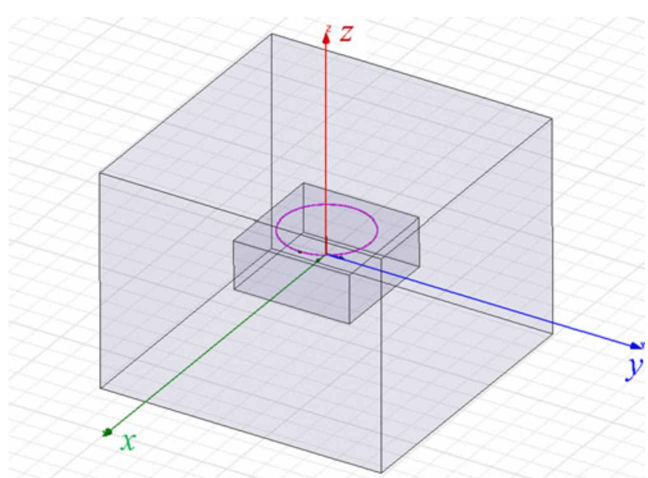

Fig. 13 Geometry of the loop antenna together with the axis system and the computation domain

In Table 1, the radiation efficiency is defined as the ratio of the radiated power to the accepted power which is the actual power delivered to the antenna on its input port. The radiation efficiency varies from 30% to 50% depending of the model. This variability is due to the phantoms morphology and especially to the body mass index (BMI) which has a strong influence on the absorbed power (see [16]).

The path loss is given in Fig. 5 for two parallel dipoles located at 30 cm from each other on each side of the chest (Fig. 1). In free space, the attenuation is about 18 dB at 900 MHz. The path loss is affected by the presence of the body which value is increased by 12.5±2.5 dB compared to the free-space case.

4.2 Miniaturized narrow-band antennas for on–on applications

4.2.1 Comparison of three miniaturized antennas

This section investigates the influence of the human body on three small antennas which could be easily integrated and printed on fabric to realize wearable structures [17]. These antennas are sensitive to both linear polarizations and have miniaturized ground planes to suit BAN applications at 2.4 GHz.

In our design methodology, BAN antennas are first manufactured without taking into account the body influence. Then the body effect on antenna matching is studied. In BAN applications, the distance between antenna and body is not necessarily controlled. Therefore it is important to analyze the antenna performances at various distances. HFSS™ is used to design three different low-profile antennas realized on FR4 substrate (relative permittivity: ε_r=4.4, loss tangent: tan δ=0.02), i.e., PIFA, IIFA (integrated inverted-F antenna), and CWPA (coplanar-wire patch antenna) described in Figs. 6, 7, and 8. Inverted-F radiating structures are chosen as they are found to be more efficient than other conventional low-profile antennas (inverted-L, mini-whip).

These three structures are characterized by a tuning short-circuit, balancing the antenna capacitance. The current is mainly concentrated in and around the short circuit. The matching bandwidths (with respect to $|S_{11}|$<10 dB) range from 5% for the PIFA and CPWA to 20% for the IFA.

Efficiency measurements of antennas in free space are based on the Wheeler cap method [18, 19] using cylindrical metallic cavities (radius=4 cm, height=2 cm). Results are comparable to numerical HFSS™ efficiency values (Table 2). It is difficult to measure the antenna efficiency

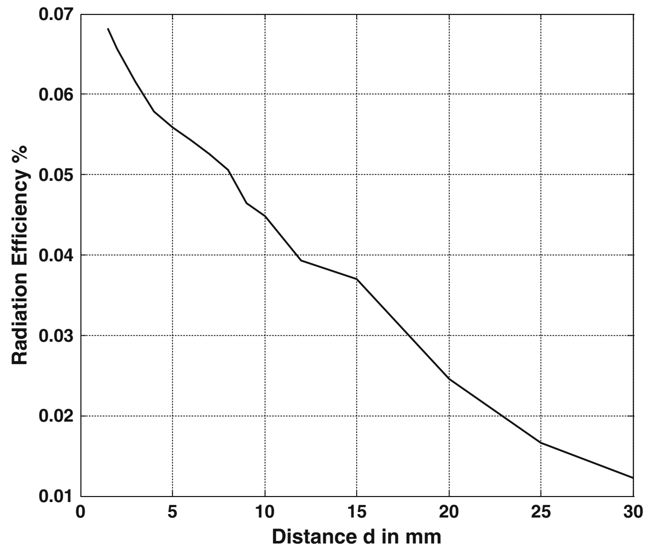

Fig. 15 Variation of the radiation efficiency of the implanted loop with its penetration into the biological tissue at 420 MHz

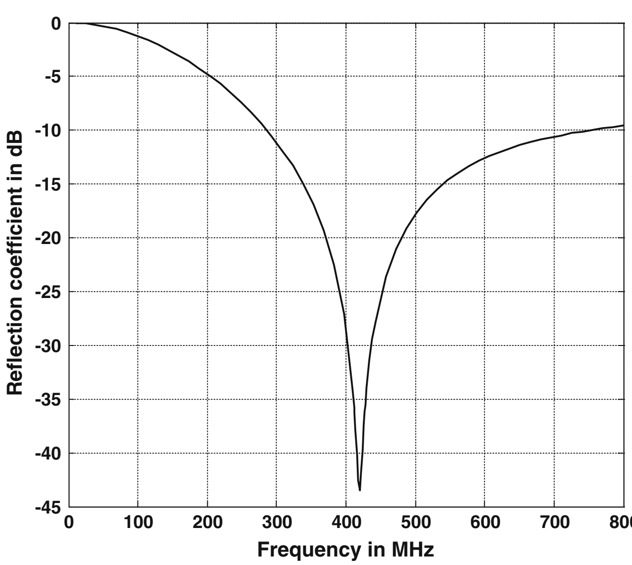

Fig. 14 Reflection coefficient versus frequency for a loop antenna embedded in a lossy human tissue at 5 mm from the slab surface

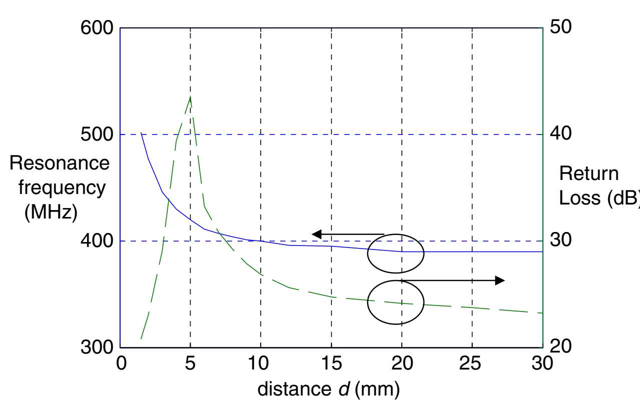

Fig. 16 Resonant frequency and return loss of the implanted loop versus its penetration into the biological tissue

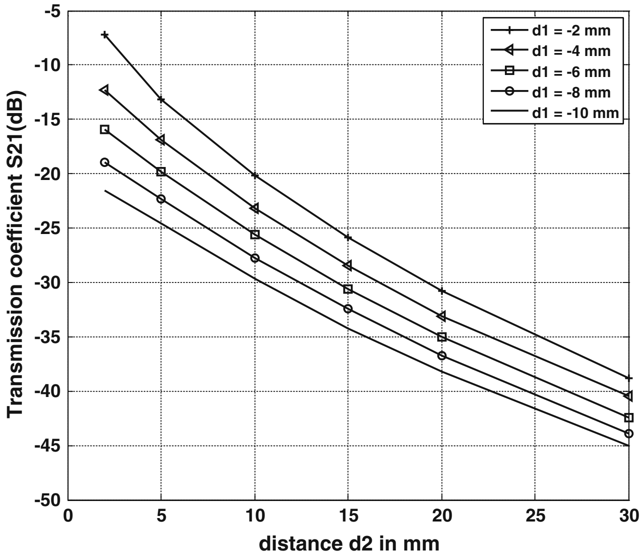

Fig. 17 Transmission coefficient $|S_{21}|$ as a function of the distance between the external loop and the body, for different positions of the implanted antenna

above body using a Wheeler cap. Therefore all efficiency values in the presence of the body have been extracted from HFSS™ simulations. The human arm (numerical) phantom is a planar multi-layered structure (Fig. 9) representing the skin, fat, muscle, and cortical bones of the arm [20].

To investigate the body influence on antennas, the phantom is introduced and simulations are performed at different distances from it: 0, 2, 4, 8 to 16 mm. For each configuration, the resonant frequency is compared with the resonant frequency in free space.

Measurements are carried out by placing the antennas on a human arm. Figure 10 shows the measured effect on the resonant frequency shift for all antennas. The PIFA is slightly affected because its near field is concentrated above the ground plane. On the other hand, CWPA and IIFA have their radiating elements co-linear to the ground plane and facing the phantom. So their characteristics are strongly affected by the human body. The matching properties of IIFA operating at 2.4 GHz in free space are shown in Fig. 11. When the antenna approaches the body, the resonance frequency slightly moves to upper values, from 2.4 to 2.6 GHz. The bandwidth also widens because of the RF losses inside the body. When the antenna gets closer to body the resonant frequency decreases resulting in a mismatch at 2.4 GHz (curve for h=3 mm, in Fig. 11).

4.2.2 Antenna desensitization—introduction of a ferrite sheet

The presence of a backing ground plane is beneficial to mask the body and limits its influence on the antenna impedance. However, low profile and integration into fabrics are the ultimate goals for most BAN applications. Therefore, a backing ground plane associated with very thin dielectric substrates (<0.5 mm) would result in inefficient, narrow-bandwidth antennas, especially for low frequencies.

Attempts are made to reduce the body influence, by introducing a 0.5 mm thick polymeric ferrite sheet (PFS) at the backside of the antenna. The ferrite surface exactly fits the antenna dimensions. The PFS characteristics are ε_r'=90, ε_r''=7, μ_r'=1 and μ_r''=6 [21]. From these characteristics, the antennas are redesigned using HFSS™ to resonate at 2.4 GHz. Following are renewed dimensions for each antenna:

- IIFA: l=4.5 mm d=3 mm and s=2 mm
- CWPA: l_p=6.5 mm and L_p=12 mm, L=46 m, l=24 mm, W_c=1.5 mm, s=1.5 mm, e=3 mm and d=1.5 mm

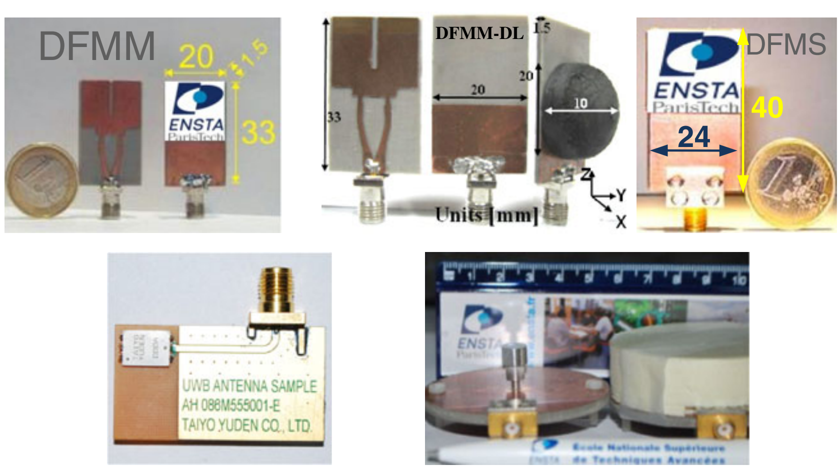

Fig. 18 Considered antennas for comparison

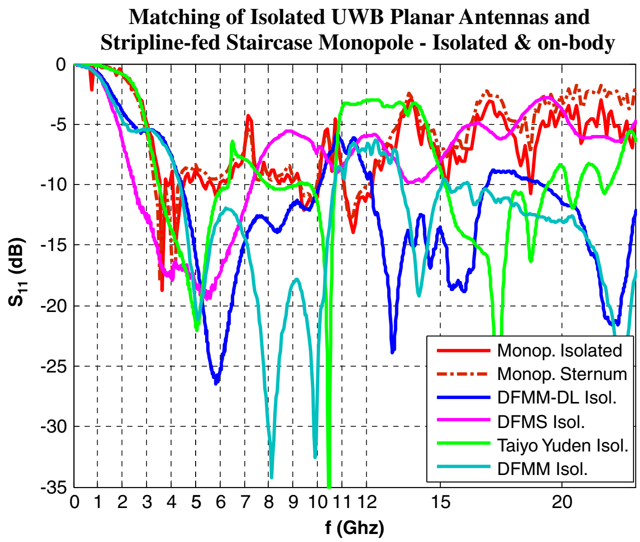

Fig. 19 Comparison of input matching and bandwidth for several isolated UWB antennas

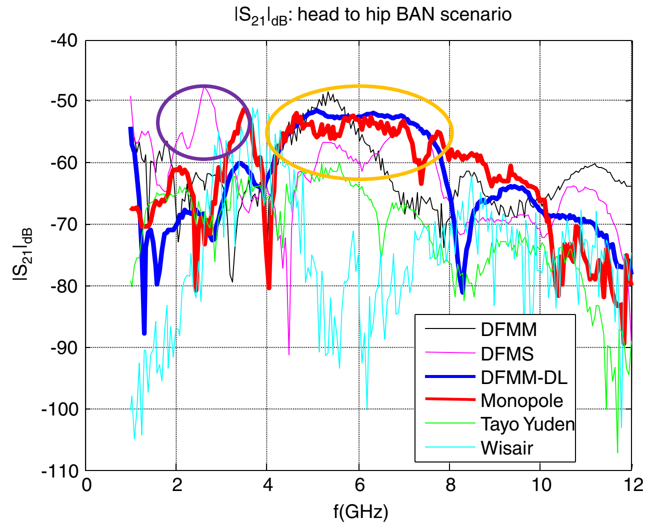

Fig. 21 Comparison of antenna performance in a head-to-hip scenario

– PIFA: since this antenna is not significantly affected by the body proximity (Fig. 10), there is no need to redesign it.

Ferrites add losses to the antenna, lowering the efficiency and increasing the bandwidth of the antenna observed in free space. Efficiency values of IIFA computed in the presence of polymeric ferrite sheets (15%) are slightly better than those obtained directly on the human arm phantom (8%). However this technique also leads to a significant reduction of the body influence (proximity and tissue dispersion) on the resonant frequency by masking the body.

CWPA measurements with and without the presence of ferrite are shown in Fig. 12. It is found that PFS acts as an efficient isolator as it reduces the influence of body (distance and tissue dispersion) on the antenna resonant frequency to a great extent. Therefore, PFS are successful in fixing the resonant frequency which is one of the main requirements for on-body applications. The same conclusions can be drawn for the IIFA in the presence of ferrite.

4.3 Implanted loop antennas for in–on applications at 400 MHz

In medical applications, rectangular and circular loop antennas are used to transmit data between external and

Fig. 20 "Statistical" dispersion of the DFMM input matching due to the body influence

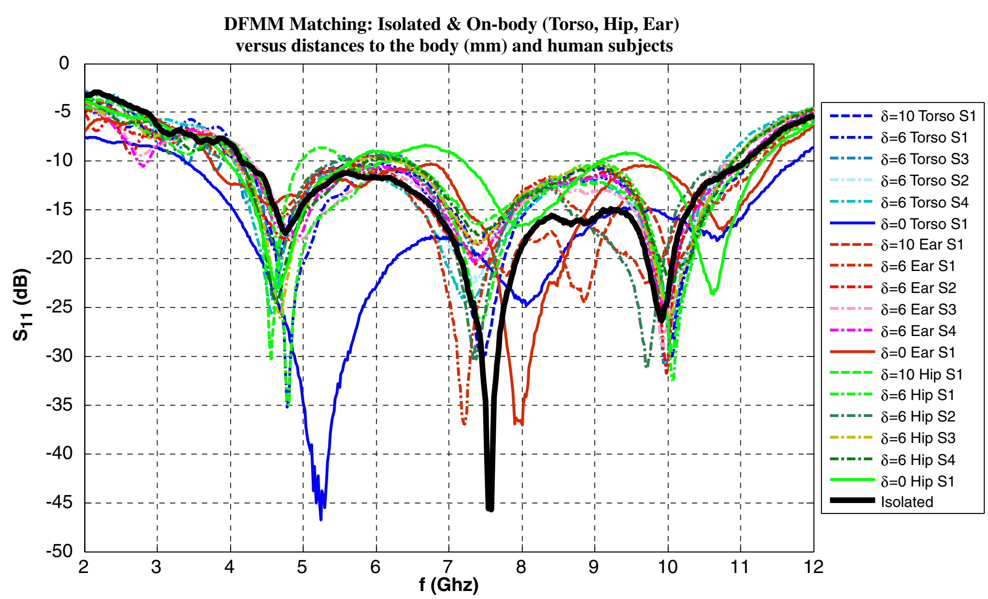

Fig. 22 Sketch of the planar balanced dipole and prototype

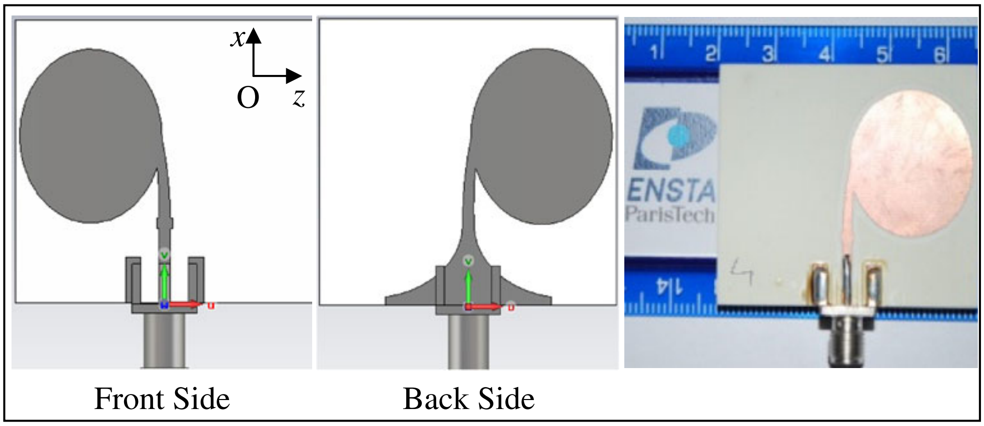

implanted devices [22–24]. In this sub-section, we investigate the effect of human tissues on the electrical parameters of a loop antenna. Moreover the transmission between a loop antenna placed above the body and a loop implanted inside the human tissues is addressed. The frequency band under consideration is the MICS band (402–405 MHz).

A circular resonating loop antenna inside human body has been simulated in HFSS (Fig. 13). Biological tissues are represented by the inner box. The simplified biological tissue model consists of a dielectric slab whose dimensions are 240×240×200 mm. Herein, an equivalent lossy dielectric with dielectric permittivity ε_r=43.9, electric conductivity σ=0.87 S/m, and a mass density ρ=1.0326 g/cm^3 is considered (according to the standardization of the International Electrotechnical Commission [25]). A miniaturization effect of the human tissue on the antenna dimensions is clearly obtained, as the radius of the resonant loop in free space is 114.5 mm to be compared with 10 mm when embedded in the human tissue.

The reflection coefficient of the implanted loop is reported in Fig. 14 for a 5 mm distance from the slab surface (z=0). The resonance is close to 420 MHz. The structure is highly lossy as indicated by the low reflection coefficient observed for frequencies above resonance. This is confirmed by a severe degradation of the antenna radiation efficiency which can be lower than 0.07%, as shown in Fig. 15. The radiation efficiency decreases monotonically with the implantation depth. These efficiencies are in good agreement with those of 0.078% given in [26]. For the same antenna dimensions, the radiation efficiency is 30% in free space.

Figure 16 presents the variation of the resonant frequency versus the antenna distance to the slab surface. The resonant frequency decreases when the antenna is moved from the surface to the body center. For small distances, typically less than 5 mm, the frequency decrease is very important. For larger distances from the surface (d> 18 mm), the resonance frequency remains almost constant, i.e., the body is seen as an infinite medium if the antenna is far enough from the surface. Figure 16 also shows that return loss values larger than 20 dB are obtained whatever the distance to the surface. This is due to the large bandwidth characteristics of the antenna resulting from high losses.

Figure 17 shows the transmission coefficient for various distances of the antennas from the body surface. The transmission coefficient is estimated for a resonant loop antenna implanted in the human body and a second one in the external region. The external loop resonates in air for a 114.5-mm radius. Comparing the considered range of distances (2 to 30 mm) to the wavelength at 400 MHz—which is of the order of 11 cm in the homogeneous tissue and 75 cm in free space—it is clear that both antennas operate in their respective near-field range, where the higher multipole terms of the field (1/r^2, 1/r^3,…, r being the distance to the antenna) dominate. The power transmis-

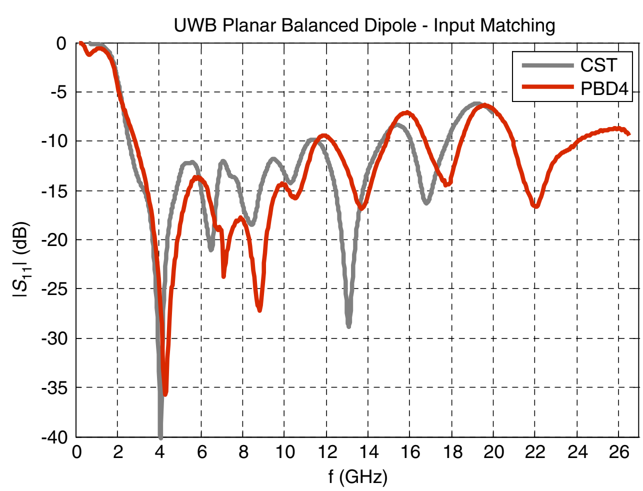

Fig. 23 Simulated and measured (“PBD4”) input matching

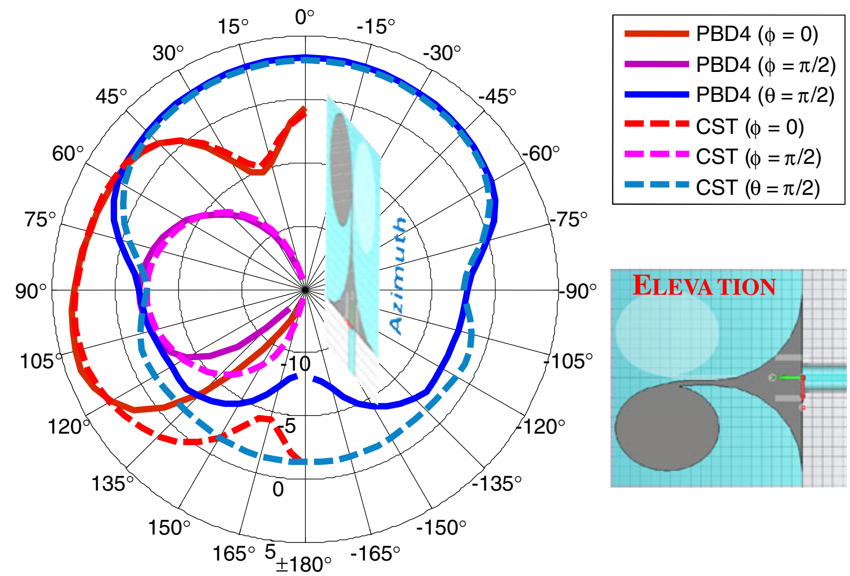

Fig. 24 Mean Realized Gain (3–13 GHz) principal cuts of the planar balanced dipole; CST® and measured (*PBD4*)

sion decreases monotonically with the antenna spacing which could help establishing a path loss model for the channel as done in [27].

If we consider an embedded loop antenna located 50 mm below the surface and an external loop located 25 mm above the surface, the $|S_{21}|$ parameter is lower than 70 dB. To have reasonable attenuations, both antennas should be placed at distances not greater than 5 mm from each side of the body surface, i.e., $d_1<5$ mm and $d_2<5$ mm.

5 BAN antennas for UWB applications

5.1 Transmission comparison for various UWB antennas

Various UWB laboratory prototypes or commercial planar or low-profile antennas (Fig. 18)—with a natural polarization tangent to the body—have been compared, focussing on their radio link performance for a few scenarios. As an example, results of a head-to-hip scenario are presented below. Input matching of isolated antennas is shown in Fig. 19 for assessing their respective typical

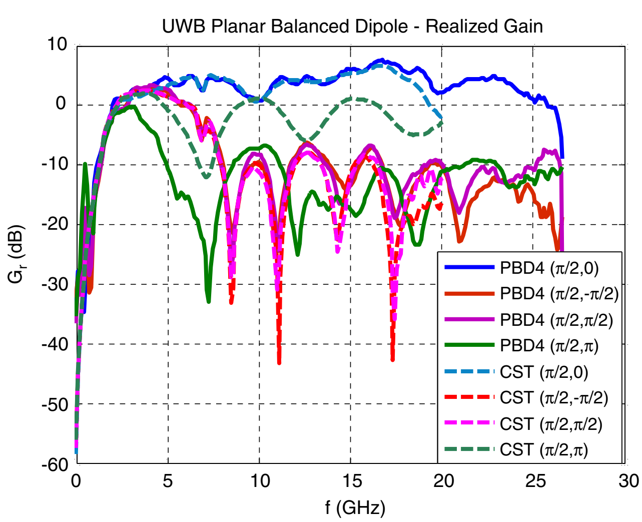

Fig. 25 Realized gain (frequency response) for the 4 cardinal directions in the equatorial plane of the measured (*PBD4*) and simulated (CST®) planar balanced dipole. The main beam direction is (θ, φ)=(π/2,0)

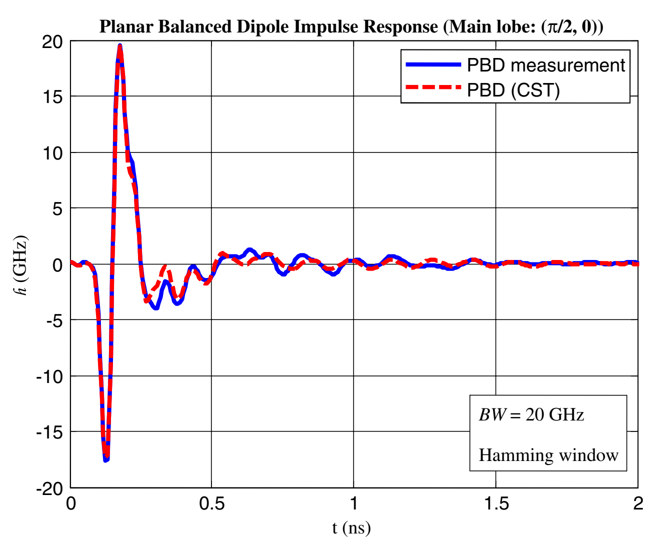

Fig. 26 Measured and simulated (CST®) PBD IR in the main beam direction (θ, φ)=(π/2,0)

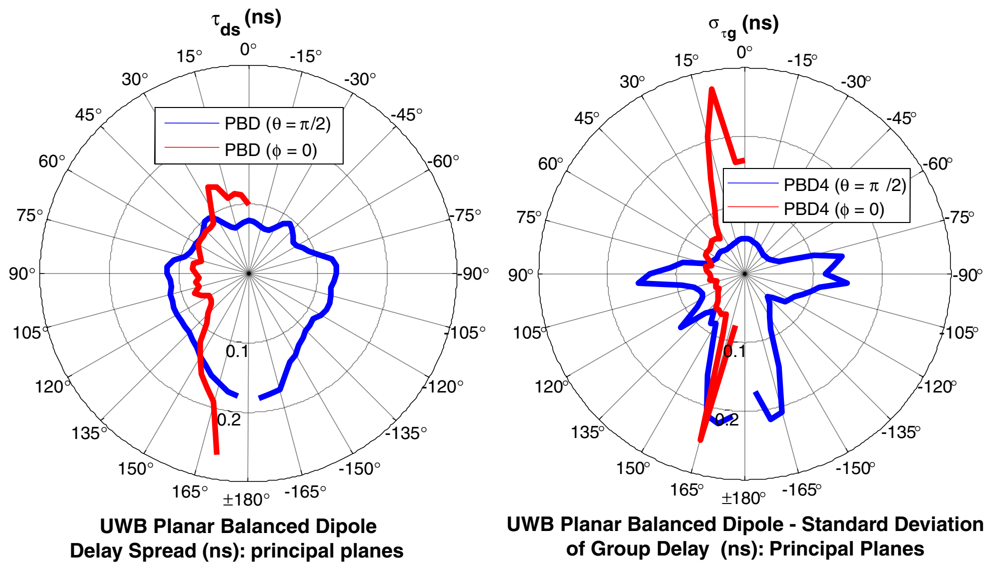

Fig. 27 Measured antenna delay spread and standard deviation of the group delay in the principal planes

input bandwidths. A stripline-fed staircase monopole, i.e., a "protruding" antenna—but with low-profile (less than 1 cm height)—with a natural polarization normal to the body has been added for comparison and conclusion in the sequel. Its reflection coefficient in situ (here at the sternum level) is also shown to demonstrate the efficient screening effect of its ground plane, at least from the matching viewpoint.

The input reflection coefficient of a dual-fed monopole in microstrip technology (DFMM) [28, 29] for various scenarios (torso, hip, ear) and parameters (distance to the body, human subject) is also provided (Fig. 20) to justify the choice of the evaluation of the input bandwidths from the isolated S_{11}. Note that Fig. 20 should be read "as a whole" (not in detail) to evaluate the statistical dispersion due to the body influence. As was previously pointed out, although the proximity of the body may locally impact significantly the return loss, its effect is of second order as regards the overall power transfer (from the source to radiation), which is first driven by the power accepted by the antenna (which remains always significant here), in particular in the case of Impulse Radio (IR) for which a broadband instantaneous bandwidth is used.

It appears clearly (Fig. 21) that in the 1.5–3-GHz frequency range, it is the dual-fed monopole in stripline technology (DFMS) [30] which outperforms the others, whereas in the 4–8-GHz range it is the dual-fed monopole in microstrip technology, with hemispherical dielectric lens (DFMM-DL) [31, 32] and the staircase monopole

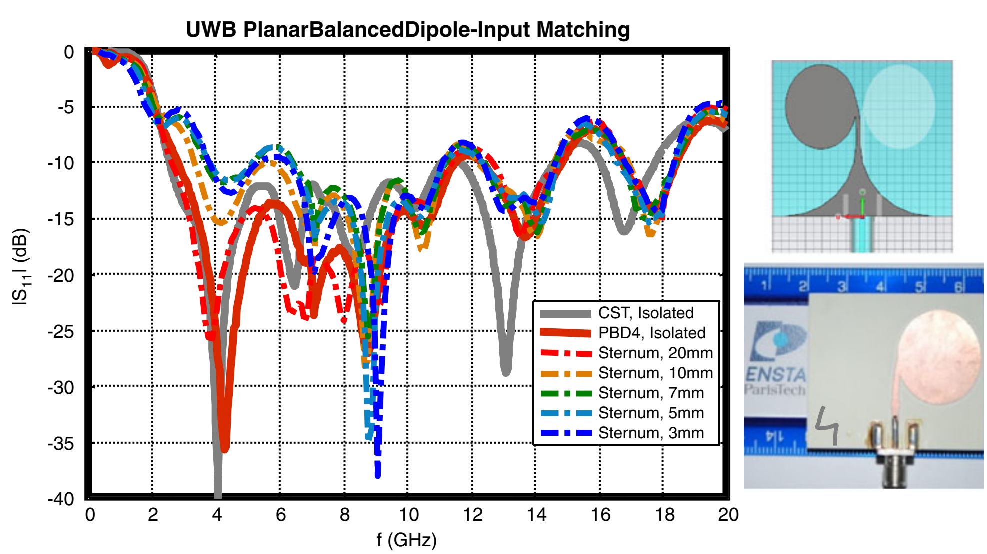

Fig. 28 Input matching at the sternum position for several antenna–body separations

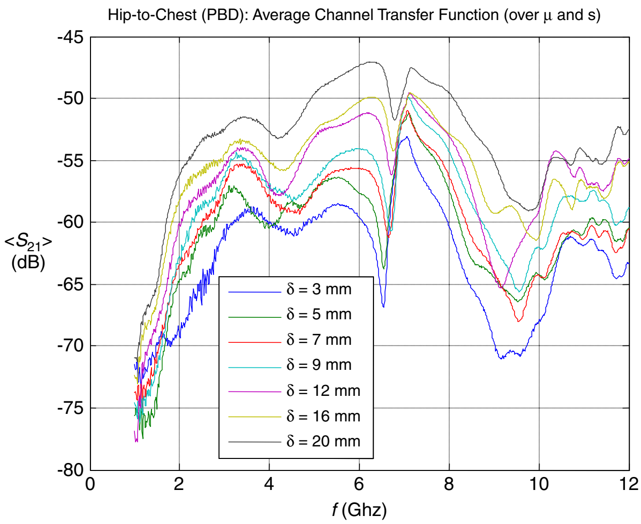

Fig. 29 Averaged measured transfer function (over µ and *s*) for the Hip-to-Chest Scenario in the anechoic chamber with δ as parameter

which behave almost identically. For the DFMS it is due to its size which is slightly higher (than the DFMM) and the fact that its feeding part (in stripline technology) is electromagnetically isolated. For the DFMM-DL, the hemispheric dielectric "lens" favors the radiation not only off the body (which provides the positive effect of reducing the antenna–body "coupling") but also in the antenna plane, i.e., along the body, which slightly improves the radio link budget. Eventually, the performance of the staircase monopole is mainly due to its intrinsic (isolated) input bandwidth (beyond ~4 GHz), the screening effect of the ground plane (of significant size, Ø, 5 cm) playing efficiently its role and the fact that the normal polarization generally outperform the tangential ones.

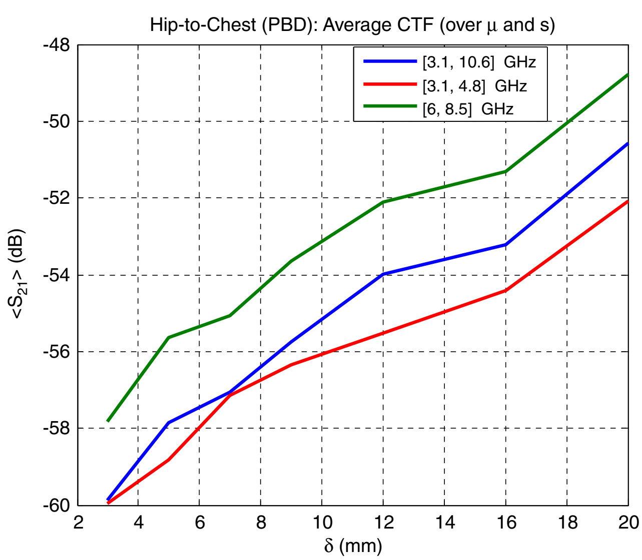

Fig. 30 Transmission as a function of antenna–body separation (extracted from results of Fig. 29, averaging over various standard bands)

5.2 UWB balanced dipoles

It is well-known (and experimentally demonstrated in the companion paper [1]) that small planar or semi-planar antennas, nor balanced nor clearly grounded are prone to potential strong "cable effects" due to common mode currents. These currents might alter the validity of the channel characterization [1] and the measurement of antenna radiation patterns. It is why UWB planar (or quasi-planar) balanced antennas have been developed: a planar balanced dipole (PBD) has been simulated with CST®, prototyped and measured at ENSTA-ParisTech and a folded semi-planar dipole, the ALVA, at CEA-Leti.

5.2.1 UWB planar balanced dipole

An UWB PBD has been designed and optimized with CST® (Fig. 22). The main goal was to minimize the size under the constraint of an input bandwidth ($|S_{11}|<10$ dB) beyond 3 GHz.

Results for the isolated antenna are first presented. The 10 dB input bandwidth is about 2.9–15 GHz, and from 2.2 to more than 26.5 GHz for a −6 dB threshold (Fig. 23). A good agreement between simulation and measurement is observed.

The mean realized gain (MRG*)* is given by:

$$\mathrm{MRG}(\hat{\mathrm{r}}) = \langle G_r \rangle = \frac{1}{\mathrm{BW}_i} \int_{f_1}^{f_2} G_r(\hat{\mathrm{r}}, f)\, df \qquad (1)$$

Its copolar θ-component is computed over a 3–13-GHz bandwidth. Measured and simulated (CST®) radiation patterns for the three principal planes (*xOy*, *xOz*, and *yOz*) are presented (Fig. 24). It can be seen that the main lobe direction is $(\theta, \varphi)=(\pi/2, 0)$, i.e. the direction opposite to the connector in the azimuthal plane. The MRG is presented in Fig. 25 as a function of the frequency for several directions of interest.

The observed discrepancies between measurement and simulation are mainly due to the masking effect of the measurement apparatus ("blind" solid angle due to the positioner head). However, in a very large solid angle around the main lobe, the agreement is excellent both directionally and in frequency. It is also noticed that the Time-Domain characteristics are excellent with a very short IR: the envelope full width at half maximum in the main lobe is less than ~90 ps with a short time ringing (~300 ps) of small amplitude (Fig. 26). More globally, the antenna delay spread or the standard deviation of the

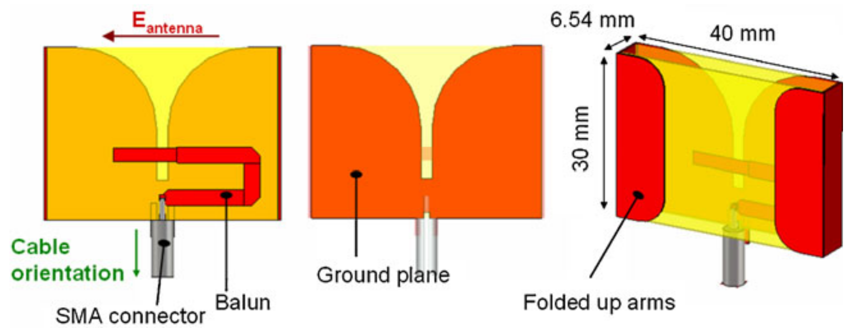

Fig. 31 ALVA antenna design

group delay [33] is less than ~100 ps in the main lobe (Fig. 27). The antenna distortion effect is consequently negligible with respect to the dispersion of the on-body channel. However, these curves should be considered with care, as they are assessed for the isolated antenna, although the close proximity of the body would impact them. Nonetheless, the antenna response cannot be deconvolved from the channel one, which means that the correct approach is to compare antennas performance regarding both power transfer and time spreading using the channel responses for each scenario (in the same conditions).

The input matching is first presented (Fig. 28). As expected, according to section 5.1, the antenna is less sensitive to the proximity effect of the subject: the trend is a monotonic decreasing with δ with an influence almost negligible for a separation beyond 20 mm.

Following the body-worn antenna characterisation in reflection, its behavior is then analyzed in transmission along the body, i.e., for two-antenna radio link configurations. The hip to chest scenario has been chosen and measurements have been performed for a fixed position of the "central node" antenna on the hip and a variable positioning ("micro-local statistics") and antenna–body separation δ (parametric analysis) on the chest. The inter-antenna distance is left constant (d=36 cm here), as well as the antenna–body separation of the central node (δ_0=20 mm).

In practice, eight "micro-positions" have been considered along a circle arc, starting from the "standard" chest position, at the sternum level, towards the left arm with sampling steps of 1.5 cm. A set of antenna–body separation distances δ has been considered. For each configuration, ten measures (VNA sweeps) have been recorded. The results presented below are averaged over the micro-positions and frequency sweeps.

Using transmission data from Fig. 29, it is shown in Fig. 30 that, on average, the attenuation is a quasi-monotonic decreasing function of the antenna–body separation, whatever the averaging bandwidth.

5.2.2 Folded semi-planar dipole (ALVA antenna)

The starting point of the antenna design is a classical notch antenna with reduced ground plane. Nevertheless the reduction of the ground plane yields a radiating behavior similar to a short circuited printed dipole antenna. Thus the ground plane acts as dipole arms at half-wavelength (λ/2).

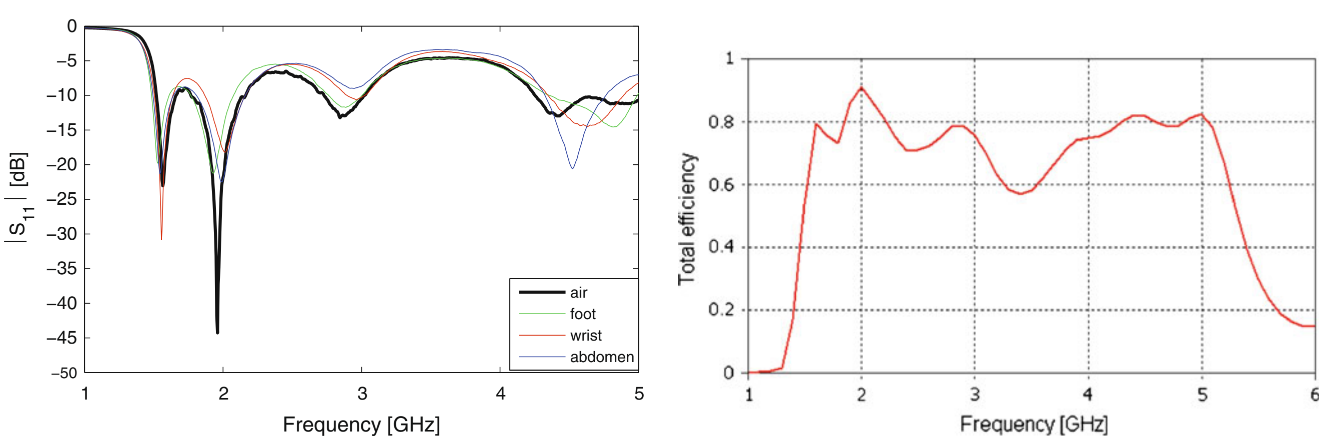

Fig. 32 ALVA antenna $|S_{11}|$ (*left*) and total efficiency (*right*)

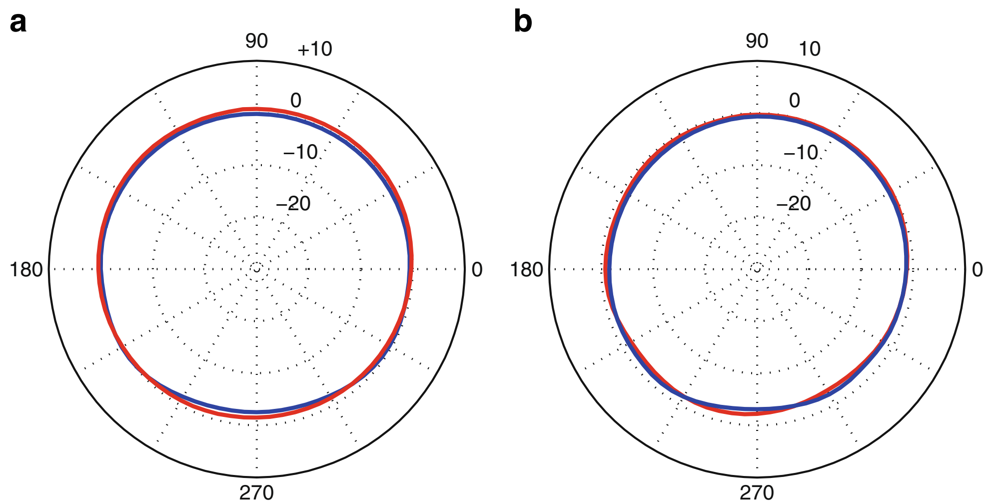

Fig. 33 ALVA mean realized gain: **a** [1.5–3] GHz, **b** [1.5–5] GHz. Measure with RF cable (*blue*) and optic link (*red*)

Since the printed dipole presents a relatively small bandwidth, the notch design has been modified in order to achieve a wideband behavior. This is obtained by means of an elliptical shape of the dipole arms, which results into a larger notch.

As a consequence the wideband impedance matching is obtained by combining two different antenna modes: in the first octave the antenna acts as dipole, with omnidirectional characteristics in the azimuth plane; while at highest frequencies the notch acts as an aperture antenna with small directive characteristics.

Additional antenna size reduction is obtained by folding up the dipole arms, which leads to a miniaturization factor of λ/5 instead of λ/2. A prototype (named ALVA) has been realized on FR4 substrate of 0.8 mm thickness (Fig. 31).

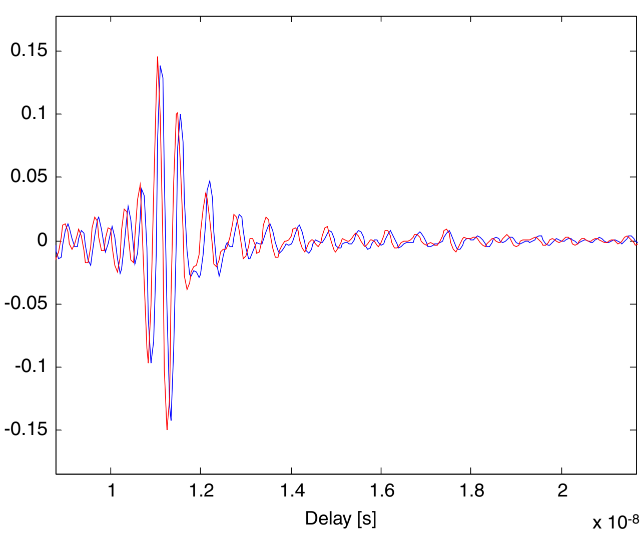

Fig. 34 Antenna impulse response: measure with RF cable (*blue*) and optic link (*red*)

The antenna reflection coefficient has been measured in "on-air" and "on-body" conditions, as depicted in Fig. 32. This antenna was originally designed to work in the 1.53.1-GHz band ($|S_{11}|$<7 dB). Nevertheless it can be employed up to 5 GHz if a slightly higher mismatch can be accepted ($|S_{11}|$<6 dB), since the antenna presents good performance in terms of total efficiency. Figure 32 shows a total efficiency larger than 75% in the 1.55 GHz, with except of a small dip at 60% in the 3.23.7-GHz band.

One of the main issues in small antenna characterization is the influence of the RF cable. This parasitic effect can sensibly affect the channel characterization. To avoid these phenomena, the ALVA design presents a Balun structure, which allows the use of a SMA connector placed on the plane of the dipole structure. At the same time the SMA connector and RF cable orientation are orthogonal to the antenna radiated field, thanks to the Balun design.

A cable-less test bed has been set up to characterize the radiation pattern of small antennas. The test bed is based on a fiber optic link. A transmitter optical sub-assembly converts RF signal to an optical one. Then a receiver optical sub-assembly converts the optical signal into a RF feed to the antenna under test.

The angle-dependent transfer function, $H(f, \theta, \varphi)$, of the ALVA antenna has been measured by using the optic link and the classical RF cable, in order to highlight the influence of the parasitic effect due to the cable.

Given the large bandwidth of the antenna, the Mean Realized Gain MRG (θ_0, φ) is computed in the azimuth plane $\theta_0=\theta_0$. Figure 33 shows the MRG measured with both methods for two different bandwidths: from 1.5 to 3 GHz and from 1.5 to 5 GHz. The antenna presents good omnidirectional characteristics in both bands. Nevertheless the poor impedance matching at higher frequencies yields to a slight gain decrease, as observed in Fig. 33b.

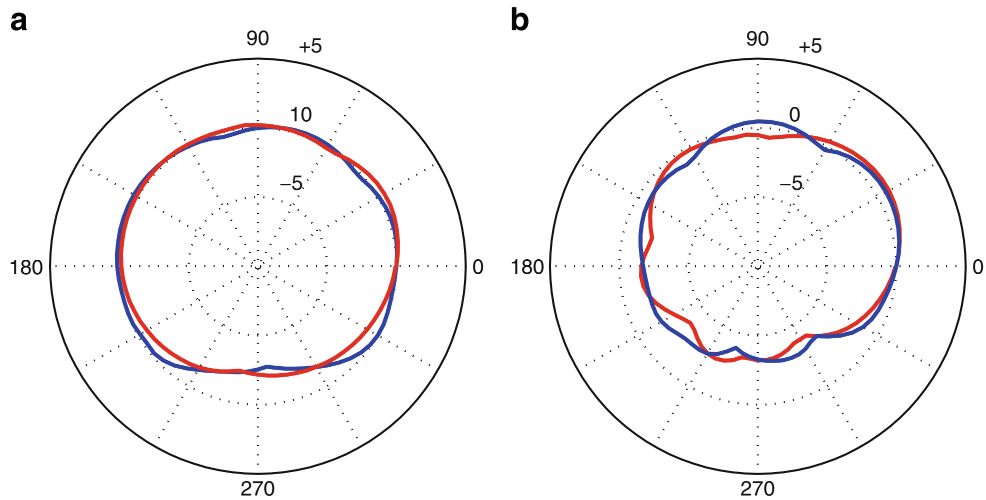

Fig. 35 Distortion factor: **a** 1.53 GHz, **b** 1.55 GHz. Measured with RF cable (*blue*) and optical link (*red*)

The most important outcome is that the differences between the RF cable and optic link measurements are practically irrelevant. This result shows that the ALVA antenna is notably a good candidate for on-body channel sounding, avoiding RF cable parasitic effect [34–36].

Figure 34 shows the antenna impulse response in the 1.53-GHz band, obtained from the measurements with RF cable and optic fiber, in the $\varnothing$=0° direction. For both, measurements present low distortion characteristics.

In order to evaluate the angular-dispersion characteristic, the distortion factor is computed as follows:

$$DF(\theta,\phi) = \frac{\max_\tau \lfloor R_{\mathrm{rec,ref}}(\tau,\theta,\phi) \rfloor}{R_{\mathrm{ref,ref}}(0,\theta,\phi)} \tag{2}$$

where $R_{i,j}(\tau) = \int_{-\infty}^{\infty} h_i(\tau) h_j(t-\tau)dt$ represents the cross correlation function between the signals $h_i(t)$ and $h_j(t)$. In the computation of the distortion factor, we used as a reference signal the antenna impulse response at $(\theta_0, \phi_0) = (0,0)$, i.e., $h_{\mathrm{ref}}(t) = h(t,\theta_0,\phi_0)$, while $h_{\mathrm{rec}}(t) = h(t,\theta_0,\phi)$ is the antenna impulse response at each azimuth angle. In Fig. 35, the distortion factor is depicted, in decibels, for the ALVA antenna in two different bands. In the 1.53-GHz band, the antenna presents a very low distortion in most of the azimuth directions.

6 Conclusions

The first part of this paper focused on the detuning effect of the antenna-to-body distance δ highlighted for resonant dipoles around 800–900 MHz and 2.4 GHz. In the absence of ground plane, the resonance frequency and the efficiency strongly depends on this distance. The influence of the morphology is moderate for the input impedance whereas tissue characteristics have some impact on the efficiency.

Miniaturized narrow-band antennas were designed at 2.4 GHz and characterized both numerically and experimentally in the BAN context. Experimental studies were conducted on human bodies. Emphasis was put on the low-profile features of these antennas. Measurements and simulations led with miniaturized antennas proved the usefulness of backing ground planes or magnetic absorbers to limit the body effects.

In-body simulations realized with a resonant loop indicate very weak efficiency values (lower than 0.1%) and a rapid degradation with the distance to the body surface. As a result, the link budget between an in-body loop and a transmit antenna above the body shows important variations depending on the relative antenna positions.

The presence of coaxial cables might alter the BAN channel characterization if small unbalanced antennas are used to sound the channel. Therefore, two planar UWB antennas suitable for BAN applications were developed, the PBD and the folded semi-planar dipole (ALVA). Both were characterized in the frequency and time domains. However, transmission characteristics were particularly underlined as the impedance detuning due to the body is averaged on the band and is not a key point. A linear dependence with the distance δ to the body surface was demonstrated for the path loss (in decibels) of the hip-to-chest scenario. The fact that antennas are properly balanced was emphasized by comparing measurements using optic links and RF cables with very small deviations between them.

Acknowledgments Authors would like to thank Daniel Toledano and Lara Traver for their contribution to measurement campaigns at ENSTA-ParisTech, Serge Bories for his initial contribution and Laurent Ouvry—from CEA-Leti—for his wise scientific advice, and Amir Yousuf, Franscesco Guidi, Enrique De Mur, and Nizar Malkiya for their help at ENSTA-ParisTech.

References

1. Roblin Ch, LaheurteJ-M, D'Errico R, Gati A, Lautru D, Alvès T, Terchoune H, Bouttout F. "Antenna design and channel modelling in the BAN context—part II: channel," submitted to annals of telecommunications, "special issue on body area networks applications and technologies," Springer
2. IEEE P802.15-08-0780-09-0006 (K. Y. Yazdandoost and K. Sayrafian-Pour): channel model for body area network (BAN), IEEE 802.15 Working Group Document, April 2009
3. Salonen P, Kim J, Rahmat-Samii Y (2005) Dual-band E-shaped patch wearable textile antenna. IEEE Proc. AP-S, Washington
4. Ouyang Y, Karayianni E, Chappell WJ (2005) Effect of fabric patterns on electrotextile patch antennas. IEEE Proc. APS, Washington
5. Tanaka M, Jang J-H (2003) Wearable microstrip antenna. IEEE Antennas and Propag Int Symp 2:704–707
6. Klemm M, Locher I, Troster G (2004) A novel circularly polarized textile antenna for wearable applications. 34th European Microwave Conferance (EuMC), Amsterdam, Netherlands
7. Klemm M, Troester G (2006) Textile UWB antennas for wireless body area networks. IEEE Trans Antennas Propag 54(11):3192–3197
8. Zhu S, Langley R (2007) Dual-band wearable antennas over EBG substrate. Electron Lett 43(3):141–142
9. Sanz-Izquierdo B, Miller JA, Batchelor JC, Sobhy MI (2010) Dual-band wearable metallic button antennas and transmission in body area networks. IET Microw Antennas Propag 4(2):182–190
10. Almpanis G, Fumeaux C, Fröhlich J, Vahldieck R (2009) A truncated conical dielectric resonator antennafor body-area network applications. IEEE Antennas Wirel Propag Lett 8:279–282
11. Terence SP, Chen ZN (2005) Effects of human body on performance of wearable PIFAs and RF transmission. IEEE Proc. AP-S, Washington
12. Kamarudin MR, Nechayev YI, Hall PS (2005) Performance of antennas in the on-body environment. IEEE AP-S Int. Symp, Washington
13. Alomainy A, Hao Y, Parini CG, Hall PS (2005) Comparison between two different antennas for UWB on-body propagation measurements. IEEE Antennas Wirel Propag Lett 4(1):31–34
14. See TSP, Chen ZN (2009) Experimental characterization of UWB antennas for on-body communications. IEEE Trans Antennas Propag 57(4):866–874
15. Ackerman MJ (1995) Accessing the Visible Human Project. DLib Mag [Online]. Available at http://www.nlm.nih.gov/research/visible/visible_human.html
16. Conil E, Hadjem A, Lacroux F, Wong MF, Wiart J (2008) Variability analysis of SAR from 20 MHz to 2.4 GHz for different adult and child models using finite-difference time-domain. Phys Med Biol 53:1511–1525
17. Alves T, Augustine R, Quéffélec P, Grzeskowiak M, Poussot B, Laheurte J-M (2009) Polymeric ferrite-loaded antennas for on-body communications. Microwave Opt Technol Lett 51(11):2530–2533
18. Newman EH, Bohley P, et Walter CH (1975) Two Methods for the Measurement of Antenna Efficiency. IEEE Transactions on Antennas and Propagation, Vol. 23, No. 4
19. Salim T, Hall PS (2006) Efficiency measurement of antennas for on-body communications. MOTL 48(11):2256–2259
20. Gabriel S, Lau RW, Gabriel C (1996) The dielectric properties of biological tissues: II. Measurements in frequency range 10 Hz to 20 GHz. Phys Med Biol 41:2251–2269
21. Baker-Jarvis J, Vanzura EJ, Kissik WA (1990) Improved technique for determining complex permittivity with the transmission/reflection method. IEEE Trans Microwave Theory Tech 38(8):1096–1103
22. Chen W-T, Chuang H-R (1998) Numerical computation of the EM coupling between a circular loop antenna and a full-scale human-body model. IEEE Trans Microwave Theory Tech 46(10):1516–1520
23. Chen W-T, Chuang H-R (1998) Numerical computation of human interaction with arbitrarily oriented superquadratic loop antennas in personal communications. IEEE Trans Antennas Propag 46 (6):821–828
24. Chen ZN, Liu GC, See TSP (2009) Transmission of RF signals between MICS loop antennas in free space and implanted in the human head. IEEE Trans Antennas Propag 57(6):1850–1854
25. www.iec.ch/
26. Hall PS, Hao Y (2006) Antennas and propagation for body-centric wireless communications. Artech House, Boston
27. Alomainy A, Hao Y (2009) Modeling and characterization of biotelemetric radio channel from ingested implants considering organ contents. IEEE Trans Antennas Propag 57:999–1005
28. Ghannoum H, Bories S, D'Errico R (2006) Small-size UWB planar antenna and its behaviour in WBAN/WPAN applications. IEE Seminar on Ultra Wideband Systems, Technologies and Applications, London, Apr. 20
29. Ghannoum H: Etude conjointe antenne/canal pour les communications Ultra Large Bande en présence du corps humain, Doctorat ENST et ENSTA, Dec. 2006 pastel.paristech.org/2083/
30. Bories S, Ghannoum H, Roblin C (2005) Robust planar stripline monopole for UWB terminal applications. Proc. 2005 IEEE International Conference on Ultra-Wideband
31. D'Errico R, Ghannoum H, Roblin Ch, Sibille A (2006) "Small Semi Directional Antenna for UWB Terminal Applications," First European Conference on Antennas and Propagation, EuCAP'06, Nice, 6–10 Nov
32. Roblin Ch, Sibille A, Bories S (2005) Semi-directional small antenna design for UWB Multimedia Terminals. ANTEM 2005 Proceedings, St. Malo, pp.142–143
33. Roblin Ch, Bories S, Sibille A (2003) Characterization tools of antennas in the time domain. IWUWBS, Oulu
34. Demeestere F, Delaveaud C, Keignart J, Bories S (2006) Compact dipole for low frequency band UWB applications. First European Conference on Antennas and Propagation, 2006. EuCAP 2006, Nice France, 6–10 Nov 2006
35. Demeestere F, Delaveaud C, Keignart J (2006) A compact UWB antenna with a wide band circuit model and a time domain characterization. IEEE International Conference on Ultra-Wideband, Waltham, MA, 24–27 Sept 2006
36. D'Errico R, Ouvry L (2009) Time-variant BAN channel characterization, PIMRC 2009, Tokyo, Japan, 13–16 Sept
37. Soras C, Karaboikis M, Tsachtsiris G, Makios V (2002) Analysis and design of an inverted-F antenna printed on a PCMCIA card for the 2.4 GHz ISM Band. IEEE Antennas and Propagation Magazine 44, No. 1
38. Huynh M-C, Stutzman W (2003) Ground plane effects on planar inverted-F antenna (PIFA) performance. IEE Proc Microw Antennas Propag 150, No. 4
39. Pasquet F, Jecko B (2001) New developments of the wire-patch antenna for ceramic technology and multifunction applications. IEEE Antennas and Propagation Society International Symposium
40. I.G. Zubal, C.R. Harrell, E.O. Smith, A.L. Smith (1995) Two dedicated voxel-based anthropomorphic (torso and head) phantoms. Proceedings of the International Workshop: Voxel Phantom Development, NRPB Chilton, UK, pp 105–111
41. Dimbylow PJ (1996) The development of realistic voxel phantoms for electromagnetic field dosimetry. Proc Int. Workshop on Voxel Phantom Development (National Radiological Protection Board Report), pp. 1–7
42. Nagaoka T, Watanabe S, Sakurai K, Kunieda E, Watanabe S, Taki M, Yamanaka Y (2004) "Development of realistic high-resolution whole-body voxel models of Japanese adult males and females of average height and weight and application of models to radio-frequency electromagnetic field dosimetry". Phys Med Biol 49:1–15